Ezrin, a membrane cytoskeletal cross-linker, is essential for the regulation of phosphate and calcium homeostasis

Ryo Hatano[1], Eiko Fujii[1], Hiroko Segawa[2], Kenichi Mukaisho[3], Mitsunobu Matsubara[4], Ken-ichi Miyamoto[2], Takanori Hattori[3], Hiroyuki Sugihara[3] and Shinji Asano[1]

[1]Department of Molecular Physiology, College of Pharmaceutical Sciences, Ritsumeikan University, Kusatsu, Japan; [2]Department of Molecular Nutrition, Institute of Health Biosciences, University of Tokushima Graduate School, Tokushima, Japan; [3]Department of Pathology, Shiga University of Medical Sciences, Seta Tsukinowa-cho, Otsu, Japan and [4]Division of Molecular Medicine, Center for Translational and Advanced Animal Research, Tohoku University School of Medicine, Sendai, Japan

Ezrin cross-links plasma membrane proteins with the actin cytoskeleton. In the kidney, ezrin mainly localizes at the brush border membrane of proximal tubules with the scaffolding protein, Na^+/H^+ exchanger regulatory factor (NHERF) 1. NHERF1 interacts with the sodium/phosphate cotransporter, Npt2a. Defects in NHERF1 or Npt2a in mice cause hypophosphatemia. Here we studied the physiological role of ezrin in renal phosphate reabsorption using ezrin knockdown mice (*Vil2*). These mice exhibit hypophosphatemia, hypocalcemia, and osteomalacia. The reduced plasma phosphate concentrations were ascribed to defects in urinary phosphate reabsorption. Immunofluorescence and immunoblotting indicated a marked reduction in renal Npt2a and NHERF1 expression at the apical membrane of proximal tubules in the knockdown mice. On the other hand, urinary loss of calcium was not found in *Vil2* mice. Plasma concentrations of 1,25-dihydroxyvitamin D were elevated following reduced plasma phosphate levels, and mRNA of the vitamin D–dependent TRPV6 calcium channel were significantly increased in the duodenum of knockdown mice. Expression of TRPV6 at the apical membrane, however, was significantly decreased. Furthermore, tibial bone mineral density was significantly lower in both the adult and young *Vil2* mice. These results suggest that ezrin is required for the regulation of systemic phosphate and calcium homeostasis *in vivo*.

Kidney International (2012) **83,** 41–49; doi:10.1038/ki.2012.308; published online 15 August 2012

KEYWORDS: calcium; phosphate uptake; vitamin D

Correspondence: *Shinji Asano, Department of Molecular Physiology, College of Pharmaceutical Sciences, Ritsumeikan University, 1-1-1 Noji-Higashi, Kusatsu, Japan. E-mail: ashinji@ph.ritsumei.ac.jp*

Received 27 October 2011; revised 11 July 2012; accepted 12 July 2012; published online 15 August 2012

Systemic P_i homeostasis is rigorously regulated in the brush border of the renal proximal tubule via the reabsorptive actions of the sodium-dependent P_i transport system. The P_i reabsorption system is mainly constituted of two members of the SLC34 family of transporters in the kidney, Npt2a and Npt2c.[1,2] In the adult rodent kidney, Npt2a has a dominant role in P_i reabsorption, and its functional membrane expression is dynamically regulated by various stimuli such as parathyroid hormone (PTH) and low P_i diet.[2,3] Npt2a has a motif in the intracellular C-terminal tail, which allows it to interact with the scaffold protein, Na^+/H^+ exchanger regulatory factor (NHERF) 1. This interaction helps in the assembly of Npt2a and the PTH receptor in the same microdomain of the apical membrane of proximal tubules.[4–6] Binding of PTH to its receptor leads to the dissociation of Npt2a from NHERF1, which initiates internalization of Npt2a. Shenolikar *et al.*[7] demonstrated that NHERF1 knockout mice exhibit abnormal expression of Npt2a in their proximal tubules and consequent hypophosphatemia. These data indicate that NHERF1 is required for the appropriate membrane localization of Npt2a. NHERF1 also interacts with ezrin, which acts as a cross-linker between NHERF1 and the actin cytoskeleton.[8,9] The functional interaction between Npt2a/NHERF1 and ezrin has been described in several *in vitro* experiments, and is controversial.[10,11] Nashiki *et al.*[10] suggests that PTH stimulates the phosphorylation of ezrin. This in turn promotes recruitment of the phosphorylated ezrin into the microdomain, which leads to the endocytosis of Npt2a.[10] In contrast, Mahon[11] suggests that coexpression of ezrin with Npt2a and NHERF1 induces the functional expression of Npt2a in the apical domain. In addition to the controversy between Np2ta/NHERF and ezrin *in vitro*, the physiological role of ezrin in the regulation of P_i transport remains unclear.

To determine the physiological role of ezrin *in vivo*, ezrin knockout mice were generated; however, it was reported that they did not survive past weaning.[12] To overcome the mortality of these knockout mice, Tamura *et al.*[13] generated

ezrin knockdown (*Vil2*$^{kd/kd}$) mice in which the expression of ezrin was downregulated to only 7% when compared with the wild-type (WT) mice. *Vil2*$^{kd/kd}$ mice also showed high mortality up to the weaning period as evidenced by a 20% survival rate within 1 month after birth; however, among those that survived, 7% of *Vil2*$^{kd/kd}$ mice survived into adulthood. *Vil2*$^{kd/kd}$ mice that survived into adulthood exhibited growth retardation and achlorhydria, as previously reported.[13] In the present study, we focused on the physiological roles of ezrin in the regulation of P_i and calcium homeostasis *in vivo*.

RESULTS

Hypophosphatemia is involved with hyperphosphaturia in *Vil2*$^{kd/kd}$ mice

Vil2$^{kd/kd}$ mice showed high mortality up to the weaning period; there was an approximate 80% mortality rate within 1 month after birth. Adult *Vil2*$^{kd/kd}$ mice that survived were analyzed for the measurement of plasma concentration levels of P_i, calcium, and other substances (Table 1). At 6–8 weeks of age, *Vil2*$^{kd/kd}$ mice exhibited significantly lower plasma concentration levels of P_i and calcium compared with WT mice (Table 1). In contrast, the urinary concentration of P_i increased threefold in *Vil2*$^{kd/kd}$ mice compared with WT mice. This was despite having found no differences in the urinary excretion of calcium between WT and *Vil2*$^{kd/kd}$ mice (Table 1).

Table 1 | Biochemical parameters in plasma and urine

	WT (*n*=10, 6–8 weeks)	*Vil2*$^{kd/kd}$ (*n*=8–10, 6–8 weeks)
Plasma		
P_i, mg/dl	9.5 ± 0.5	6.1 ± 0.6[a]
Ca^{2+}, mg/dl	10.5 ± 0.5	8.6 ± 0.5[a]
$1,25(OH)_2$ vitamin D, pg/ml	201.9 ± 32.5	479.7 ± 97.6[a]
PTH, pg/ml	20.2 ± 1.6	19.3 ± 1.1
Urine		
P_i, mg/mg creatinine	1.06 ± 0.14	2.99 ± 0.63[a]
Ca^{2+}, mg/mg creatinine	0.11 ± 0.12	0.08 ± 0.02
Uric acid, μg/mg creatinine	3.76 ± 0.49	6.91 ± 3.12
Glucose, mg/mg creatinine	0.11 ± 0.02	0.04 ± 0.02
Total excreted P_i, mg/day	2.5 ± 0.3	6.1 ± 0.3[a]
Total excreted Ca^{2+}, mg/day	0.073 ± 0.019	0.067 ± 0.013
FEP_i, %	3.23 ± 0.46	16.6 ± 2.4[a]
FECa, %	0.31 ± 0.03	0.32 ± 0.04
FEGlu, %	0.012 ± 0.003	0.010 ± 0.002

Abbreviations: FECa, fractional excretion index of calcium; FEGlu, fractional excretion index of glucose; FEP_i, fractional excretion index of P_i; PTH, parathyroid hormone; WT, wild-type.
[a]$P<0.05$, vs. WT mice.

The fractional excretion indexes of P_i (FEP_i) and Ca (FECa) were analyzed using 24-h urine samples and calculated using the equation described in Materials and Methods. FEP_i significantly increased to 16.6 ± 2.4% in *Vil2*$^{kd/kd}$ mice (WT mice: 3.23 ± 0.46%), whereas FECa was unchanged (WT mice: 0.31 ± 0.03%, and *Vil2*$^{kd/kd}$ mice: 0.32 ± 0.04%). These results suggest that the hypophosphatemia shown in *Vil2*$^{kd/kd}$ mice is caused by the urinary loss of P_i, possibly attributed to abnormal reabsorption of P_i in the proximal tubules.

No obvious histological differences between WT and *Vil2*$^{kd/kd}$ mice were found in hematoxylin and eosin–stained kidney sections (Supplementary Figure S1 online). In the WT mouse kidney, immunofluorescence analyses revealed positive staining for ezrin, which was predominantly observed in the apical membrane of proximal tubules and in the glomeruli (Figure 1a). In addition, ezrin colocalized with NHERF1 and Npt2a at the apical membrane of proximal tubules (Supplementary Figure S2a and b online). However, in *Vil2*$^{kd/kd}$ mice, the expression of ezrin was suppressed almost completely (Figure 1b), and subcellular localization of NHERF1 and Npt2a was altered compared with WT mice. Moreover, the apical staining for Npt2a was markedly reduced in the proximal tubule of *Vil2*$^{kd/kd}$ mice, and positive staining was exclusively found in the intracellular compartment (Figure 1f). In *Vil2*$^{kd/kd}$ mice, higher-magnification images demonstrated that Npt2a did not colocalize with radixin. Npt2a localized to the subapical region and intracellular vesicle compartments, whereas radixin localized to the apical membrane of proximal tubules (Figure 1g). Some Npt2a staining was found in intracellular vesicle compartments, specifically colocalizing with the Golgi marker protein, GM130 (Figure 1g). Coincidently, NHERF1 was also observed in the intracellular compartments in the proximal tubules of *Vil2*$^{kd/kd}$ mice (Figure 1d), where GM130 was localized (Figure 1h). Furthermore, NHERF1-positive staining was also found in the subapical region. This staining pattern was similar to that of Npt2a. However, some parts of NHERF1 colocalized with radixin at the apical membrane of proximal tubules (Figure 1d and h). On the other hand, localization of other members of the ERM (ezrin–radixin–moesin) proteins, radixin and moesin, which were also expressed in the apical membrane of proximal tubules in WT mice, were not altered in *Vil2*$^{kd/kd}$ mice (Supplementary Figure 2c and d online). These results suggest that abnormal localization of both Npt2a and NHERF1 is attributable, in part, to the decreased expression level of ezrin. It is also likely

Figure 1 | Localization of ezrin, NHERF1, and Npt2a in wild-type (WT) and *Vil2*$^{kd/kd}$ mouse kidneys. The immunofluorescence analyses for (**a**, **b**) ezrin, (**c**, **d**) NHERF1, and (**e**, **f**) Npt2a were performed in (**a**, **c**, and **e**) WT and (**b**, **d**, and **e**) *Vil2*$^{kd/kd}$ mouse kidneys. (**a**) The expression of ezrin was observed mainly in the apical membrane of proximal convoluted tubules (PCTs) and in the glomeruli (G) of the WT mouse kidney. (**b**) In contrast, ezrin staining markedly diminished in the *Vil2*$^{kd/kd}$ mouse kidney. (**c**, **e**) NHERF1 and Npt2a exclusively localized to the apical membrane of the PCT in WT kidneys. (**d**, **f**) However, in the *Vil2*$^{kd/kd}$ mouse kidney, the apical localization of these proteins was reduced, and an additional positive staining was observed in the intracellular compartments. The images represent × 200 magnification and the scale bar represents 50 μm. (**g**, **h**) In the *Vil2*$^{kd/kd}$ mouse kidney, the intracellular localizations of Npt2a and NHERF1 were examined by triple staining with radixin and a Golgi apparatus marker protein, GM130 (× 600). White arrows indicate subapical localization of Npt2a or NHERF1, and yellow arrowheads indicate colocalization of GM130 and Npt2a or NHERF1. The scale bar represents 10 μm.

that radixin and moesin do not compensate for the loss of ezrin in the proximal tubules.

We further confirmed the expression level of Npt2a and NHERF1 in the brush border membrane vesicle (BBMV) fraction of proximal tubules and in the total lysate of kidney cortex by immunoblotting. The purity of the BBMV fractions from WT mouse kidneys was checked by immunoblotting against membrane proteins that are specifically expressed in

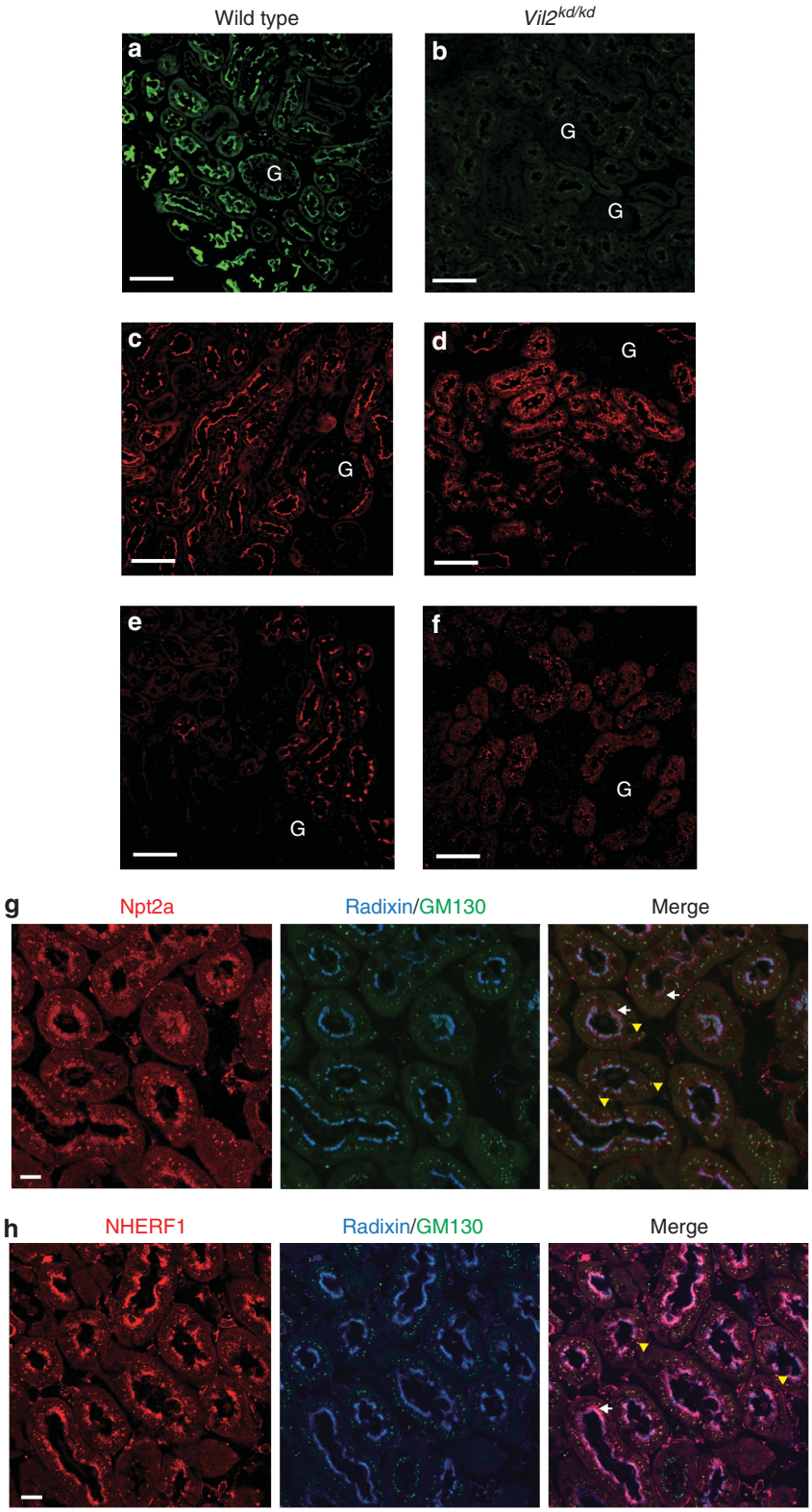

the brush border membrane of proximal tubules. These include villin-1 and MRP4, which were highly expressed (three to four times greater compared with total cell lysate samples) in the BBMV fractions (Supplementary Figure S3 online). GM130 (a marker protein for the Golgi apparatus) and GAPDH (glyceraldehyde-phosphate dehydrogenase; a marker protein for cytoplasm) were not detected in BBMV fractions, suggesting that the fractions did not contain intracellular compartments such as the Golgi apparatus and cytoplasm (Supplementary Figure S3 online). In *Vil2*$^{kd/kd}$ mice, ezrin expression was almost completely suppressed in the total lysate of kidney cortex and the BBMV fraction (Figure 2). The total amounts of Npt2a and NHERF1 in the total lysate were not different between WT and *Vil2*$^{kd/kd}$ mice (Figure 2a). However, the expression levels of these proteins in the BBMV fraction were markedly reduced in *Vil2*$^{kd/kd}$ mice. In addition, the expression levels of villin-1 and β-actin in the BBMV fraction were not different between WT and *Vil2*$^{kd/kd}$ mice (Figure 2b). The densitometric analyses of immunoblotting for Npt2a and NHERF1 in the BBMV fractions demonstrated that the expression levels of Npt2a and NHERF1 in the BBMV fractions of *Vil2*$^{kd/kd}$ mice were reduced by 89 ± 4% and 79 ± 8% compared with WT mice, respectively (Figure 2c). We also investigated the expression levels of other ERM proteins in the total lysate of kidney cortex. Total amounts of radixin and moesin were not different between WT and *Vil2*$^{kd/kd}$ mice (Figure 2). These results were consistent with those found in the immunofluorescence analyses. In addition, the expression level of Npt2c in the BBMV fraction was also significantly reduced in *Vil2*$^{kd/kd}$ mice. The expression level of Npt2c in the total lysate of kidney cortex was much lower than that of Npt2a, but not different between WT and *Vil2*$^{kd/kd}$ mice, as in the case of Npt2a and NHERF1.

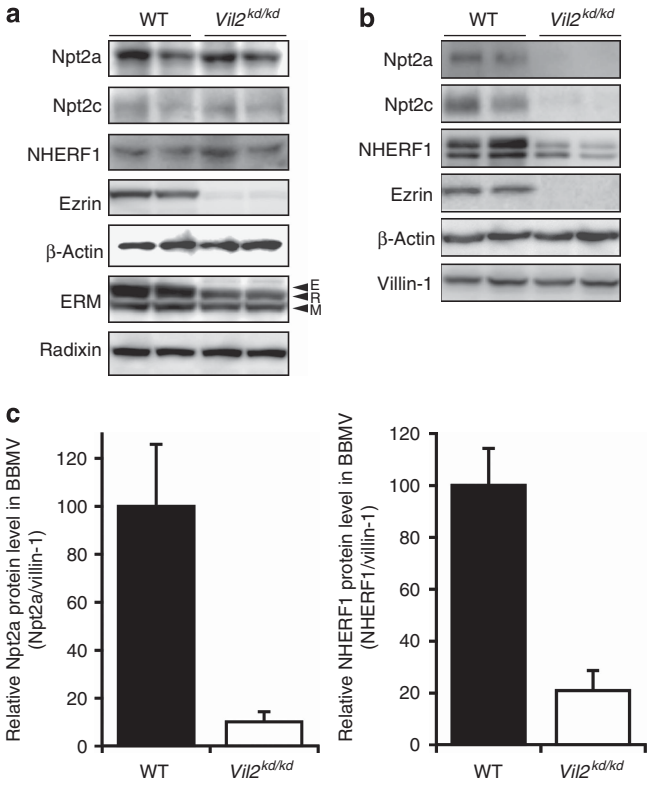

Figure 2 | Immunoblotting of the total lysate of kidney cortex and brush border membrane vesicle (BBMV) fraction. (**a**) To determine the total protein expression in the kidney cortex, the total renal cortical lysate was used. Although a significant difference between the wild-type (WT) and *Vil2*$^{kd/kd}$ mouse was observed for the total expression of ezrin, none was observed for the total expression of Npt2a, Npt2c, NHERF1, moesin, and radixin. Arrowheads indicate the band corresponding to the expected molecular weight of ezrin (E), radixin (R), and moesin (M), respectively. The upper band contains ezrin and radixin, which were difficult to separate via sodium dodecyl sulfate–polyacrylamide gel electrophoresis. The expression levels of radixin were confirmed using an antibody specific for radixin. (**b**) The expression levels of these proteins were also examined in the BBMV. Ezrin and Npt2a were markedly reduced in the BBMV of the *Vil2*$^{kd/kd}$ mouse kidney; however, faint bands corresponding to the NHERF1 and Npt2a proteins were observed. The expression levels of villin-1 and β-actin in the BBMV were not statistically different between WT and *Vil2*$^{kd/kd}$ mouse kidneys. (**c**) The relative densities of Npt2a and NHERF1 to villin-1 in BBMV were quantified from immunoblots ($n = 6$–8).

Hypocalcemia is involved with the abnormal duodenal calcium absorption

Intestinal calcium absorption is critical for the regulation of systemic calcium homeostasis. Ca^{2+} is absorbed in the intestinal mucosa by the paracellular and transcellular pathways.[14] $1,25(OH)_2$ vitamin D–dependent upregulation of duodenal Ca^{2+} absorption is an important system for the maintenance of systemic Ca^{2+} balance. In the transcellular pathway, TRPV6, a member of the transient receptor potential family of calcium channel, has a predominant role in the Ca^{2+} absorption from duodenal mucosa, and TRPV6 expression depends on the plasma $1,25(OH)_2$ vitamin D level. In the present study, *Vil2*$^{kd/kd}$ mice exhibited significant hypocalcemia and no urinary loss of Ca^{2+} (Table 1). *Vil2*$^{kd/kd}$ mice also showed elevated levels of plasma $1,25(OH)_2$ vitamin D (Table 1), a similar finding that was reported in Npt2a knockout mice.[15] In addition, plasma PTH concentrations were not significantly altered in *Vil2*$^{kd/kd}$ mice. Despite the elevation of plasma $1,25(OH)_2$ vitamin D, plasma Ca^{2+} concentrations were decreased in *Vil2*$^{kd/kd}$ mice. Therefore, we examined the duodenal TRPV6 mRNA expression levels in *Vil2*$^{kd/kd}$ mice. Real-time reverse-transcription PCR demonstrated the transcriptional upregulation of TRPV6 in response to the elevated plasma 1, 25 $(OH)_2$ vitamin D in *Vil2*$^{kd/kd}$ mice (Figure 3a). This result suggests that the responsiveness of TRPV6 expression to the alteration of plasma $1,25(OH)_2$ vitamin D level was not disturbed in *Vil2*$^{kd/kd}$ mice. The responsiveness of TRPV6 expression was also confirmed by immunoblotting analyses on total lysates of duodenal mucosa (Figure 3b). We examined the localization of TRPV6 in the duodenal mucosa by immunoblotting and immunofluorescence analyses (Figures 3b, c and 4). The purity of the BBMV fractions from WT mouse duodenum

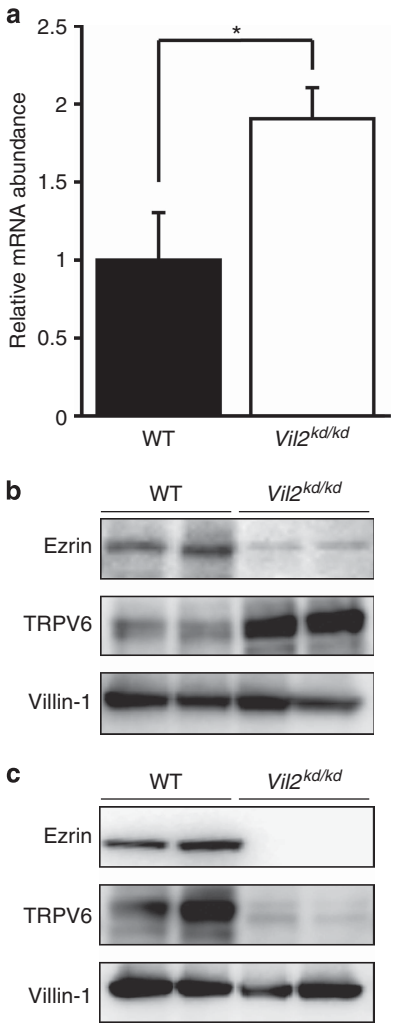

Figure 3 | Real-time reverse-transcription (RT)-PCR and immunoblotting analysis for TRPV6 in the mouse duodenum mucosa. (**a**) TRPV6 mRNA expression in the duodenum mucosa of wild-type (WT) and *Vil2*$^{kd/kd}$ mice was determined using real-time RT-PCR. TRPV6 mRNA expression was significantly increased in the *Vil2*$^{kd/kd}$ mice. Values are shown as mean ± s.e. ($n = 6$). *$P < 0.05$. The protein expression levels of ezrin, TRPV6, and villin-1 in the duodenum were examined using (**b**) the total duodenal lysate and (**c**) the brush border membrane vesicle (BBMV), respectively.

was checked by immunoblotting (Supplementary Figure S3 online). The specificity of the mouse TRPV6 antibody was confirmed by immunoblotting and immunofluorescence analyses of HEK and Caco-2 cells transiently expressed with recombinant flag-tagged mouse TRPV6 (Supplementary Figure S4 online). In WT mice, ezrin and TRPV6 were exclusively observed in the apical regions of duodenal mucosa and the BBMV fraction (Figures 3c and 4a–c). The expression level of ezrin was completely suppressed in the duodenum in *Vil2*$^{kd/kd}$ mice (Figures 3c and 4d). Both immunoblotting and immunofluorescence analyses for TRPV6 demonstrated abnormalities in duodenal TRPV6 localization. These abnormalities include reduced expression in the BBMV fraction and increased intracellular positive staining (Figures 3c and 4e). The images at higher magnification showed the intracellular localization of TRPV6 investigated by double staining with GM130. However, unlike Npt2a and NHERF1 in the *Vil2*$^{kd/kd}$ kidney, TRPV6 did not colocalize with GM130 in the duodenum of *Vil2*$^{kd/kd}$ mice. TRPV6 expression was increased in the other intracellular compartments and accumulated in the regions around goblet cells (Figure 4g).

Bone analysis in *Vil2*$^{kd/kd}$ mice

Bone mineral density (BMD) was measured by the dual-emission X-ray absorptiometry method. The right tibia was collected and analyzed. At 8 weeks of age, *Vil2*$^{kd/kd}$ mice showed significant decreases in tibial BMD levels compared with WT mice (Figure 5a). Furthermore, *Vil2*$^{kd/kd}$ mice at 3 weeks of age also showed marked reductions in the tibial BMD levels (Figure 5a). Villanueva–Goldner staining was also performed to determine the abnormality of bone mineralization in *Vil2*$^{kd/kd}$ mice. In the tibia of 4-week-old *Vil2*$^{kd/kd}$ mice, impaired bone mineralization was also observed (Figure 5b). These results suggest that *Vil2*$^{kd/kd}$ mice develop impaired bone mineralization and osteomalacia starting in early life.

DISCUSSION

Ezrin is involved in the interaction between membrane proteins and/or adaptor proteins and actin cytoskeleton. In the kidney, ezrin is dominantly expressed in the apical membrane of proximal tubules, but its physiological roles have not been fully understood. In the present study, we examined the physiological roles of ezrin in the regulation of phosphate and calcium homeostasis in the kidney using *Vil2*$^{kd/kd}$ mice.

Biochemical analyses of *Vil2*$^{kd/kd}$ mice showed significant decreases in plasma P_i and calcium concentrations in conjunction with the urinary loss of P_i but not calcium. In the proximal tubules of *Vil2*$^{kd/kd}$ mice, the apical membrane expression levels of Npt2a and NHERF1 were markedly reduced. Beck *et al.*[15] reported that Npt2a-deficient mice develop mild hypophosphatemia and urinary P_i loss; however, they did not exhibit rickets or osteomalacia because of the compensatory upregulation of Npt2c expression in these mice. Recently, Segawa *et al.*[16] reported that the double-knockout mice of Npt2a and Npt2c showed a greater severity of hypophosphatemia, hypercalciuria, and rickets compared with Npt2a knockout mice.[16] In our study, we found that *Vil2*$^{kd/kd}$ mice developed a phenotype similar to that of double knockout mice mice in that they also exhibited hypophosphatemia and rickets, but not hypercalciuria. In the proximal tubules of *Vil2*$^{kd/kd}$ mice, expression levels of Npt2c and Npt2a at the apical membrane were markedly reduced (no changes in Npt2c and Npt2a were detected in the total lysate). The defects of both P_i transporters at the apical membrane are possibly related to the abnormality of bone mineralization in *Vil2*$^{kd/kd}$ mice.

Interactions among Npt2a, NHERF1, and ezrin have been reported in *in vitro* experiments. Npt2a protein was shown to interact with a PDZ motif–binding protein, NHERF1, via its

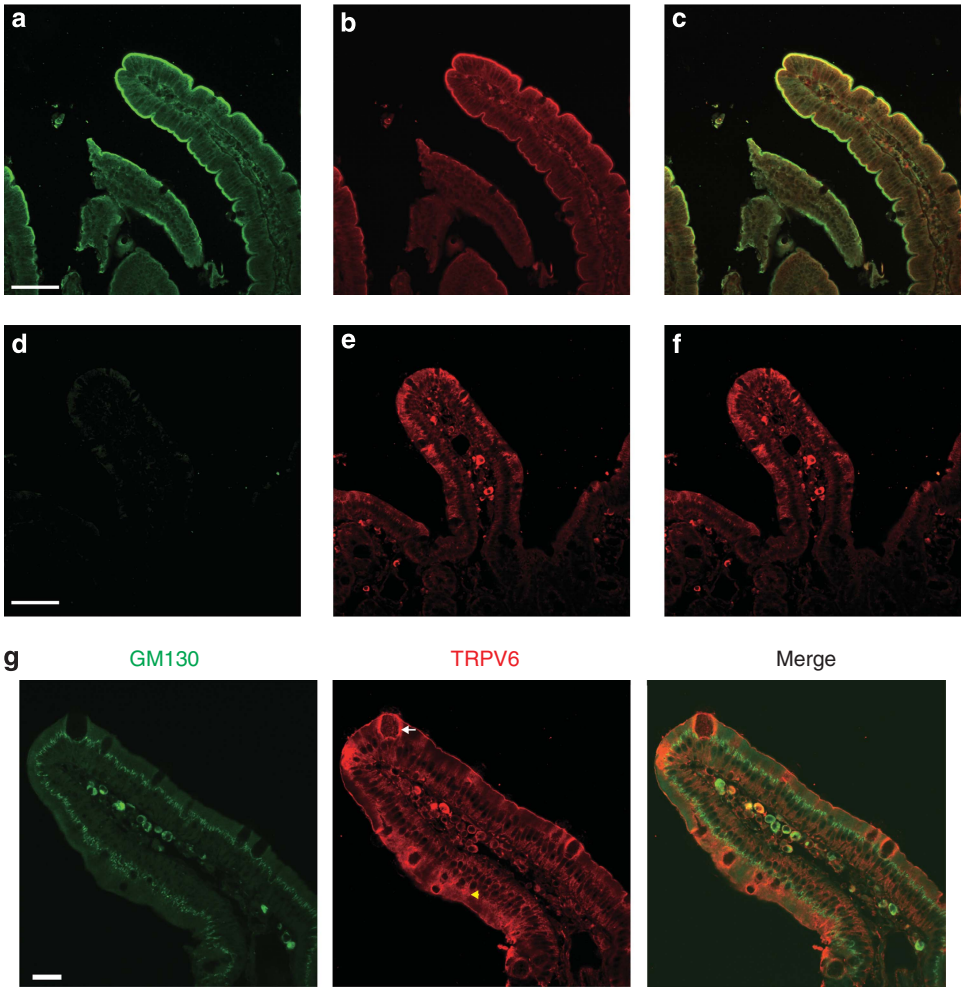

Figure 4 | Duodenal localization of ezrin and TRPV6 in *Vil2*$^{kd/kd}$ and wild-type (WT) mice. The immunofluorescence analyses for ezrin and TRPV6 were performed in the WT and *Vil2*$^{kd/kd}$ mouse duodenum. In the WT mouse duodenum, the colocalization of (**a**) ezrin and (**b**) TRPV6 was exclusively observed in a thin layer along the apical membrane of villus tips, as evidenced by the (**c**) merged images. In the *Vil2*$^{kd/kd}$ mouse duodenum, (**d**) minimal ezrin expression was detected, and (**e**) the membrane expression of TRPV6 was disturbed. The merged image of **d** and **e** is shown in **f**. The images represent $\times 400$ magnification and the scale bar represents 25 μm. (**g**) In the *Vil2*$^{kd/kd}$ mouse duodenum, the subcellular localization of TRPV6 was examined by double staining with GM130 ($\times 600$). White arrows indicate the localization of TRPV6 around goblet cells, and a yellow arrowhead indicates intracellular localization of TRPV6. The scale bar represents 10 μm.

last three C-terminal amino-acid residues TRL.[17,18] Targeted disruption of NHERF1 gene *in vivo* also led to the reduced membrane expression of Npt2a and consequent abnormal urinary loss of P_i, suggesting that NHERF1 has an important role in the apical targeting and/or trafficking of Npt2a.[7] This phenotype aligns with our observations in the *Vil2*$^{kd/kd}$ mouse. Our data suggest that in *Vil2*$^{kd/kd}$ mice the mislocalization of NHERF1 involved with ezrin knockdown may lead to a reduction in Npt2a expression at the apical membrane. On the other hand, Npt2c does not have a PDZ-binding motif in its C terminus, but is reported to interact with NHERF1 and NHERF3.[19] The mechanism underlying these interactions is unclear; however, we speculate that the mislocalization of NHERF1 may be associated with a defect in adaptive recruitment of Npt2c into the apical membrane. These results suggest that ezrin has important roles in apical membrane trafficking of transporters and scaffold proteins.

Although *Vil2*$^{kd/kd}$ mice exhibit similar phenotypes as Npt2a or NHERF1 knockout mice with regard to P_i homeostasis, they show different phenotypes in the regulation of calcium homeostasis. In Npt2a knockout mice, hypophosphatemia led to the adaptive increase in $1,25(OH)_2$ vitamin D synthesis, which in turn elicited a marked stimulation of duodenal calcium absorption.[15,20] Duodenal calcium hyperabsorption would then result in hypercalcemia and consequent hypercalciuria.[15,20] In the Npt2a knockout mice duodenum, TRPV6 mRNA expression was upregulated.[20] In *Vil2*$^{kd/kd}$ mice, however, hypercalcemia and hypercalciuria were not observed despite the adaptive increase of plasma $1,25(OH)_2$ vitamin D concentrations and upregulation of TRPV6 mRNA and protein in the

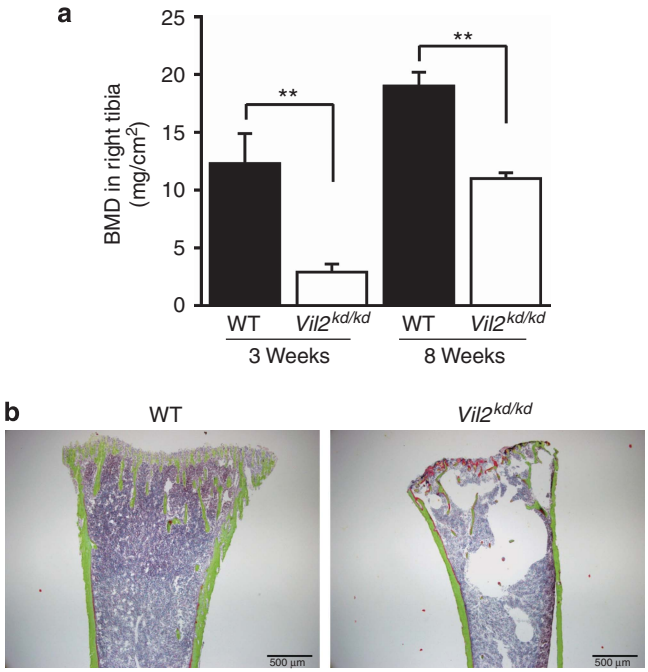

Figure 5 | Bone mineral density (BMD) analysis of *Vil2*$^{kd/kd}$ and wild-type (WT) mice. (**a**) The BMD of the right tibia of WT and *Vil2*$^{kd/kd}$ mice at 3 and 8 weeks of age was investigated using the dual-emission X-ray absorptiometry method. Each column represents the mean ± s.e. ($n = 3$). $^{**}P < 0.01$. (**b**) The representative images of Villanueva–Goldner-stained sections of right tibiae from WT and *Vil2*$^{kd/kd}$ mice. The green- and red-stained tissues denote mineralized bone and osteoid tissue, respectively.

duodenum. In the present study, we found that the membrane expression of TRPV6 was disturbed, although TRPV6 mRNA and protein expression levels were responsive to increased $1,25(OH)_2$ vitamin D in the *Vil2*$^{kd/kd}$ mice duodenum. Similar adaptive mRNA upregulation of TRPV5 was also observed in the *Vil2*$^{kd/kd}$ mice duodenum. However, the duodenal TRPV5 mRNA expression levels in *Vil2*$^{kd/kd}$ mice were still much lower than the basal TRPV5 mRNA expression level of the WT mouse kidney (WT duodenum: 0.8 ± 0.5%, and *Vil2*$^{kd/kd}$ duodenum: 5.8 ± 2.7% of WT kidney, respectively; Supplementary Figure S5 online). As reported previously by Van Cromphaut *et al.*,[21] the duodenal expression level of TRPV5 is much lower than that of TRPV6. Therefore, the transcellular Ca^{2+} uptake ability in the duodenum might be highly influenced by the changes in TRPV6 expression and its subcellular localization.

In *in vitro* experiments, the interaction between NHERF4 and TRPV5/6 via PDZ-binding domains has been reported.[22] The functional interaction between the TRPV6 channel and its binding to ezrin or NHERF-1 has not been fully explored. In this study, we determined that NHERF1 localization was disturbed in the duodenum of *Vil2*$^{kd/kd}$ mice (Supplementary Figure S6 online). Although the interaction between TRPV5/6 and NHERF1 or NHERF2 remains controversial, ezrin might regulate the membrane expression of TRPV5/6 via the interaction with NHERF1.

The phenotype of *Vil2*$^{kd/kd}$ mice in the dysfunction of phosphate and calcium regulation was different from those of Npt2a- or NHERF1-deficient mice, as described above, and from other mutant mice that have been reported for hereditary hypophosphatemic rickets.[23] The phenotype of *Vil2*$^{kd/kd}$ mice is similar to that of the vitamin D receptor knockout mice that showed rickets, hypocalcemia, hypophosphatemia, and elevated serum levels of $1,25(OH)_2$ vitamin D, except for hyperparathyroidism.[21,24] Therefore, the dysfunction of ezrin might be closely associated with hereditary vitamin D–resistant rickets.

The molecular mechanism of how ezrin regulates the membrane expression of Npt2a, Npt2c, and TRPV6 remains unclear. In the previous report, *Vil2*$^{kd/kd}$ mice exhibited severe achlorhydria caused by defects in the formation/expansion of canalicular apical membranes in gastric parietal cells.[13] Ezrin defects led to the dysfunction of the membrane fusion of gastric vesicles with canalicular membranes in parietal cells, even in the presence of histamine.[13] In the present study, our results suggest that ezrin is likely to be essential for the targeting or stabilization of several transporters, channels, and scaffold proteins onto the plasma membrane. Thus, ezrin might be associated with membrane trafficking of the intracellular vesicles containing transporters and channels.

In conclusion, we found abnormalities in P_i and calcium handling in *Vil2*$^{kd/kd}$ mice, which is attributable to a reduced membrane expression of Na^+/P_i cotransporters in the kidney and TRPV6 in the duodenum. The mislocalization of the scaffold protein NHERF1 may, in part, cause reduced expression of these transporters and channels at the apical membrane. In addition, the onset of the *Vil2*$^{kd/kd}$ phenotype is similar to hypophosphatemic vitamin D–resistant rickets. Altogether, it is clear that the mechanisms of ezrin to regulate the membrane localization of these proteins require future elucidation.

MATERIALS AND METHODS

Antibodies and reagents

Anti-ezrin antibodies were purchased from Acris Antibody GmbH (3C12, mouse monoclonal antibody, Hiddenhausen, Germany) and Cell Signaling Technology (#3145, rabbit polyclonal antibody, Danvers, MA). Rabbit anti-NHERF1 antibody was purchased from Abcam (ab3452, Cambridge, UK), and rabbit anti-TRPV6 antibody was purchased from Alomone Labs (#ACC-036, Jerusalem, Israel). Mouse monoclonal anti-β-actin antibody and goat anti-villin-1 antibody were purchased from Santa Cruz Biotechnology (sc-69879 and sc-7672, Santa Cruz, CA). Rabbit anti-ezrin–radixin–moesin polyclonal antibody and rat anti-radixin monoclonal antibody were prepared as described previously.[25] Mouse anti-GM130 antibody was purchased from BD Biosciences (558712, San Jose, CA). Anti-Npt2a and anti-Npt2c were prepared as described previously.[16] For immunofluorescence staining, a fluorescein isothiocyanate–labeled goat anti-mouse or goat anti-rat IgG, Cy5-labeled anti-rat IgG, and Alexa Fluor 594–labeled anti-rabbit antibody were used (Invitrogen, Carlsbad, CA).

Animals

Vil2$^{kd/kd}$ mice were obtained from the laboratory of Professor Sachiko Tsukita (Osaka University). *Vil2*$^{kd/kd}$ mice exhibited a high

mortality up to the weaning period, as described previously.[13] However, technical improvement in our way of handling and feeding successfully decreased the high mortality. Three- to eight-week-old sex-matched, WT and *Vil2*$^{kd/kd}$ mice were used in this study. For genotyping, genomic DNA was isolated by tail biopsy, and PCR was performed using KOD-FX polymerase (TOYOBO, Osaka, Japan) with the following primers: 5′-GTGTGGCACTCTGCCTT CAAG-3′ (forward primer for the WT allele), 5′-CATGGTGCCA CACAGGACTC-3′ (reverse primer for the WT allele), and 5′-AGCGGATCTCAAACTCTCCTC-3′ (reverse primer for the targeted allele). All work with animals was performed with approval from the Animal Ethics Committees of Shiga University of Medical Sciences and Ritsumeikan University.

To determine the urinary excretion of phosphate and other substrates, mice were placed in metabolic cages for 24 h, and were provided with standard rodent chow and water *ad libitum*. Daily water consumption, urine volume, and food intake were measured. After urine samples were collected, blood, kidney, and duodenum were collected.

Biochemical analysis of plasma and urine

Blood was obtained via heart puncture under appropriate anesthesia, and the plasma was separated by centrifugation at 1000 *g* for 10 min at 4 °C. Concentrations of plasma and urinary Ca and P_i were determined using DRI-CHEM 4000i (Fujifilm, Tokyo, Japan). The plasma and urinary concentrations of creatinine, uric acid, and glucose were also determined by DRI-CHEM 4000i. Concentrations of plasma PTH were determined using the PTH enzyme–linked immunosorbent assay kit (Immunotopics, San Clemente, CA). Concentrations of plasma $1,25(OH)_2$ vitamin D were determined by a radioimmunoassay (Medic, Shiga, Japan). Twenty-four-hour urine collections were performed as mentioned above, and the total amount of excreted substrates was measured. The FEP_i and FECa were calculated as urine P_i or Ca × plasma creatinine × 100/(urine creatinine × plasma P_i, or Ca).

Preparation of kidney and duodenum lysate and the BBMV fractions and immunoblotting analysis

Mouse kidney and duodenum BBMV fractions were isolated according to the method described by Biber *et al.*[26] Briefly, WT and *Vil2*$^{kd/kd}$ mice were anesthetized by diethyl ether and perfused through the left ventricle with 30 ml of phosphate-buffered saline (PBS) to remove all blood from the kidneys and intestine. Kidneys were rapidly harvested and the renal cortex was separated using a razor blade. The duodenum was also quickly harvested, washed with ice-cold PBS, laid open, and the mucosa was gently scraped off. Each tissue was homogenized in Lysis buffer composed of 150 mmol/l NaCl, 3 mmol/l KCl, 5 mmol/l EDTA, 3 mmol/l ethylene glycol tetraacetic acid, and 50 mmol/l Tris-HCl (pH 7.4) containing 1% Triton X-100, followed by centrifugation at 3000 *g* for 10 min for the collection of total lysate. For the isolation of the BBMV fractions, tissues were homogenized in homogenization buffer composed of 300 mmol/l D-mannitol, 5 mmol/l ethylene glycol tetraacetic acid and 12 mmol/l Tris-HCl (pH 7.1) using a Polytron homogenizer for 2 min. $MgCl_2$ solution was added into the homogenate up to 12 mmol/l. Then, the mixture was kept on ice for 15 min, and the homogenate was centrifuged at 1500 *g* for 15 min. The supernatant was collected and centrifuged at 25,000 *g* for 30 min. The pellet was resuspended in the Lysis buffer.

For immunoblotting analysis, 15–30 μg of protein was loaded into each lane for Laemmli's sodium dodecyl sulfate–polyacrylamide gel electrophoresis (8–12.5%), and then transferred to a polyvinylidendifluoride membrane. The membrane was blocked for 1 h by using 2.5% milk powder in TBST (10 mmol/l Tris-HCl, pH 8.5, 150 mmol/l NaCl, and 0.1% Tween 20), and exposed to primary antibodies diluted with Solution 1 (Can Get Signal; TOYOBO) overnight at 4 °C. After a TBST rinse, the secondary antibody diluted with Solution 2 (Can Get Signal; TOYOBO) was applied to the membrane for 1 h at room temperature. After washing, antigen–antibody complexes were visualized with a chemiluminescence system (ECL plus; GE Healthcare, Waukesha, WI).

Table 2 | A list of PCR primers

TRPV6	
Forward primer: 5′-TTGGGCTGGTGCAATGTCA-3′	
Reverse primer: 5′-AGCCAGCAGAATCGCATCAAG-3′	
Glyceraldehyde-phosphate dehydrogenase	
Forward primer: 5′-TGTGTCCGTCGTGGATCTGA-3′	
Reverse primer: 5′-TTGCTGTTGAAGTCGCAGGAG-3′	

Real-time PCR analysis

Total RNA from the mucosa of the mouse duodenum was extracted using the RNeasy Mini kit (QIAGEN) according to the manufacturer's instructions. Total RNA was reverse-transcribed using the PrimeScript RT-Reagent kit (TaKaRa Bio, Otsu, Japan), and the subsequent cDNA generated was used for quantitative real-time reverse-transcription PCR. Quantitative analyses for mouse TRPV6 and GAPDH were performed using the CYBR Premix Ex Taq (Takara Bio). The gene-specific primers to TRPV6 and GAPDH are shown in Table 2. The expression level of each mRNA was normalized to the expression level of GAPDH.

Immunofluorescence analysis

Mouse kidney and duodenum were fixed with 4% paraformaldehyde in 0.1 mol/l phosphate buffer (pH 7.4), embedded in paraffin, and then cut into thin sections (4 μm). After deparaffinization and rehydration, the sections were immersed into a 0.01-mol/l citrate buffer, and autoclaved for the activation of immunogenicity. Slides were then washed in PBS, and incubated with primary antibodies overnight at 4 °C. Next, slides were washed with PBS-T (0.1% Tween 20 in PBS) and then incubated with the secondary antibodies for 1 h at room temperature. After a final PBS-T wash, the sections were mounted with fluorescent mounting medium (DAKO, Kyoto, Japan) and examined using a confocal laser scanning microscope (FV-1000D IX-81, Olympus, Tokyo, Japan).

Bone tissue preparation

For the determination of BMD, right tibiae were removed from 3- and 8-week-old WT and *Vil2*$^{kd/kd}$ mice. The tibiae were immersed in 70% ethanol overnight, and BMD was determined by the dual-emission X-ray absorptiometry method. For Villanueva–Goldner staining, right tibiae were excised from 4-week-old WT and *Vil2*$^{kd/kd}$ mice. The tibiae were fixed with 70% ethanol, embedded in methyl methacrylate, and then cut into 6-μm sections.

DISCLOSURE

All the authors declared no competing interests.

ACKNOWLEDGMENTS

We thank Professor Sachiko Tsukita and Dr Atsushi Tamura for *Vil2*$^{kd/kd}$ mice. We also thank Dr Natasha Moningka for proofreading. This research was supported in part by a Grant-in-Aid for Scientific

Research (21590082) from the Ministry of Education, Culture, Sports, Science and Technology of Japan to SA, and a High-Tech Research Center Project for Private Universities: matching fund subsidy from the Ministry of Education, Culture, Sports, Science and Technology of Japan to SA.

SUPPLEMENTARY MATERIAL

Figure S1. Hematoxylin and eosin staining for the WT and *Vil2*$^{kd/kd}$mouse kidneys.
Figure S2. Colocalization of ezrin, NHERF1, Npt2a, moesin, and radixin in the apical membrane of the proximal tubules in WT kidney, and apical membrane expressions of moesin and radixin in *Vil2*$^{kd/kd}$ mouse kidney.
Figure S3. Purity of the BBMV examined by immunoblotting.
Figure S4. Characterization of a commercially available anti-TRPV6 antibody.
Figure S5. Adaptive up-regulation of TRPV5 in the duodenum of *Vil2*$^{kd/kd}$ mouse.
Figure S6. Abnormal expression of NHERF1 in the duodenal mucosa of *Vil2*$^{kd/kd}$ mouse.
Supplementary material is linked to the online version of the paper at http://www.nature.com/ki

REFERENCES

1. Biber J, Hernando N, Forster I *et al.* Regulation of phosphate transport in proximal tubules. *Pflugers Arch* 2009; **458**: 39–52.
2. Murer H, Hernando N, Forster I *et al.* Proximal tubular phosphate reabsorption: molecular mechanisms. *Physiol Rev* 2000; **80**: 1373–1409.
3. Forster IC, Hernando N, Biber J *et al.* Proximal tubular handling of phosphate: a molecular perspective. *Kidney Int* 2006; **70**: 1548–1559.
4. Bacic D, Wagner CA, Hernando N *et al.* Novel aspects in regulated expression of the renal type IIa Na/Pi-cotransporter. *Kidney Int Suppl* 2004; **91**: S5–S12.
5. Weinman EJ, Steplock D, Shenolikar S *et al.* Dynamics of PTH-induced disassembly of Npt2a/NHERF-1 complexes in living OK cells. *Am J Physiol Renal Physiol* 2011; **300**: F231–F235.
6. Déliot N, Hernando N, Horst-Liu Z *et al.* Parathyroid hormone treatment induces dissociation of type IIa Na^+-P(i) cotransporter-Na^+/H^+ exchanger regulatory factor-1 complexes. *Am J Physiol Cell Physiol* 2005; **289**: C159–C167.
7. Shenolikar S, Voltz JW, Minkoff CM *et al.* Targeted disruption of the mouse NHERF-1 gene promotes internalization of proximal tubule sodium-phosphate cotransporter type IIa and renal phosphate wasting. *Proc Natl Acad Sci USA* 2002; **99**: 11470–11475.
8. Bretscher A, Edwards K, Fehon RG. ERM proteins and merlin: integrators at the cell cortex. *Nat Rev Mol Cell Biol* 2002; **3**: 586–599.
9. Morales FC, Takahashi Y, Kreimann EL *et al.* Ezrin-radixin-moesin (ERM)-binding phosphoprotein 50 organizes ERM proteins at the apical membrane of polarized epithelia. *Proc Natl Acad Sci USA* 2004; **101**: 17705–17710.
10. Nashiki K, Taketani Y, Takeichi T *et al.* Role of membrane microdomains in PTH-mediated down-regulation of NaPi-IIa in opossum kidney cells. *Kidney Int* 2005; **68**: 1137–1147.
11. Mahon MJ. Ezrin promotes functional expression and parathyroid hormone- mediated regulation of the sodium-phosphate cotransporter 2a in LLC-PK1 cells. *Am J Physiol Renal Physiol* 2008; **294**: F667–F675.
12. Saotome I, Curto M, McClatchey AI. Ezrin is essential for epithelial organization and villus morphogenesis in the developing intestine. *Dev Cell* 2004; **6**: 855–864.
13. Tamura A, Kikuchi S, Hata M *et al.* Achlorhydria by ezrin knockdown: defects in the formation/expansion of apical canaliculi in gastric parietal cells. *J Cell Biol* 2005; **169**: 21–28.
14. Hoenderop JG, Nilius R, Bindels RJ. Calcium absorption across epithelia. *Physiol Rev* 2005; **85**: 373–422.
15. Beck L, Karaplis AC, Amizuka N *et al.* Targeted inactivation of Npt2 in mice leads to severe renal phosphate wasting, hypercalciuria, and skeletal abnormalities. *Proc Natl Acad Sci USA* 1998; **95**: 5372–5377.
16. Segawa H, Onitsuka A, Furutani J *et al.* Npt2a and Npt2c in mice play distinct and synergistic roles in inorganic phosphate metabolism and skeletal development. *Am J Physiol Renal Physiol* 2009; **297**: F671–F678.
17. Hernando N, Déliot N, Gisler SM *et al.* PDZ-domain interactions and apical expression of type IIa Na/P_i cotransporters. *Proc Natl Acad Sci USA* 2002; **99**: 11957–11962.
18. Gisler SM, Stagljar I, Traebert M *et al.* Interaction of the type IIa Na/P_i cotransporter with PDZ protein. *J Biol Chem* 2001; **276**: 9206–9213.
19. Villa-Bellosta R, Barac-Nieto M, Breusegem SY *et al.* Interactions of the growth-related, type IIc renal sodium/phosphate cotransporter with PDZ proteins. *Kidney Int* 2008; **73**: 456–464.
20. Tenenhouse HS, Gauthier C, Martel J *et al.* Na/P_i cotransporter (Npt2) gene disruption increases duodenal calcium absorption and expression of epithelial calcium channels 1 and 2. *Pflugers Arch* 2002; **444**: 670–676.
21. Van Cromphaut SJ, Dewerchin M, Hoenderop JG *et al.* Duodenal calcium absorption in vitamin D receptor-knockout mice: functional and molecular aspects. *Proc Natl Acad Sci USA* 2001; **98**: 13324–13329.
22. Van de Graaf SF, Hoenderop JG, Van der Kemp AW *et al.* Interaction of the epithelial Ca^{2+} channels TRPV5 and TRPV6 with the intestine- and kidney-enriched PDZ protein NHERF4. *Pflugers Arch* 2006; **452**: 407–417.
23. Alizadeh Naderi AS, Reilly RF. Hereditary disorders of renal phosphate wasting. *Nat Rev Nephrol* 2010; **6**: 657–665.
24. Li YC, Pirro AE, Amling M *et al.* Targeted ablation of the vitamin D receptor: an animal model of vitamin D-dependent rickets type II with alopecia. *Proc Natl Acad Sci USA* 1997; **94**: 9831–9835.
25. Kondo T, Takeuchi K, Doi Y *et al.* ERM (ezrin/radixin/moesin)-based molecular mechanism of microvillar breakdown at an early stage of apoptosis. *J Cell Biol* 1997; **139**: 749–758.
26. Biber J, Stieger B, Stange G *et al.* Isolation of renal proximal tubular brush-border membranes. *Nat Protoc* 2007; **2**: 1356–1359.